Journal of Mathematics and Computer Science

A new mathematical model approach on the oncolytic virotherapy potency

Check for updates

Amal T. Alshammari[a,b], Normah Maan[a,*], Mahmoud A. M. Abdelaziz[c,d]

[a]*Department of Mathematical Sciences, Faculty of Science, Universiti Teknologi Malaysia, Johor Bahru 81310, Johor, Malaysia.*

[b]*Department of Mathematics, Faculty of Science, University of Hafr Al Batin, Hafar Al Batin, Saudi Arabia.*

[c]*School of Quantitative Sciences, College of Arts & Sciences, Universiti Utara Malaysia, Kedah, Malaysia.*

[d]*Department of Mathematics, Faculty of Arts and Sciences, Najran University, Najran, Saudi Arabia.*

Abstract

In recent times, there has been an increasing focus on investigating the therapeutic capacity of virus particles in the management of cancer. This paper introduces a novel discrete-time mathematical model with fractional-order of oncolytic virotherapy. The model captures the complex behavior of how cancer cells and virus particles interact, aiming to elucidate the process of infecting and eliminating cancer cells in the absence of immune involvement. To evaluate the efficacy of cancer-targeting virus treatment, we perform an in-depth analysis of both the local stability and the bifurcation trends observed in our framework. By selecting appropriate bifurcation parameters, we verify the occurrence of codimension one bifurcations, for instance, fold, flip as well as Neimark-Sacker (N-S), as well as codimension-two flip-N-S bifurcations. The identification of these bifurcation types is established by deriving necessary and sufficient conditions using algebraic criterion methods. In these criteria, the reliance does not lie in the attributes of the eigenvalue coefficients from the characteristic equation of the Jacobian matrix but rather on the coefficients of the Jacobian matrix's characteristic equation itself. Consequently, we have semi-algebraic systems comprising equations, inequalities, and inequalities. This algebraic methodology provides appropriate conditions for both codimension one as well as codimension-two bifurcations in high-dimensional maps. Finally, numerical simulations were conducted to validate our theoretical findings. Our study concludes that the correlated increase between cancer cell proliferation and the therapeutic virus indeed resulted in the anticipated infection within the cancer cells. While complete eradication of cancer cells using viral therapy alone is not impossible, it requires specific conditions.

Keywords: Virotherapy cancer treatment, calculus involving fractional orders, model in discrete time, equilibrium stability, bifurcations, chaos.

2020 MSC: 37N25, 92C50, 35Q92.

1. Introduction

Cancer is a major global health concern, with millions of new cases each year, leading to millions of deaths [9]. The disease's complexity and variation make it difficult to choose the best treatment, dosage, and timing. Medical professionals work hard to make informed decisions to achieve the preferred

*Corresponding author

Email addresses: theyab@graduate.utm.my (Amal T. Alshammari), normahmaan@utm.my (Normah Maan), mamabdelaziz@hotmail.com; maabdelaziz@nu.edu.sa (Mahmoud A. M. Abdelaziz)

outcomes for patients, whether seeking a cure or providing palliative care. However, traditional cancer treatments often come with high toxicity, side effects, and limited effectiveness [20]. Survivors may endure late treatment effects, underscoring the necessity for safer and more effective treatments [20]. Researchers have consistently aimed to discover a treatment that not only effectively eradicates the disease but also prevents its return, in addition to continuous efforts to find treatments that do not contain side effects. The development of new systems for diagnosing and treating cancers that directly target cancer cells without affecting normal cells is essential [19]. A promising approach treatment to achieving this goal is virotherapy of cancer.

This new promising treatment has the potential to be safer and less complicated than other treatments and may work against a wide range of cancers. Oncolytic virotherapy is an advanced novel treatment for cancerous tumours that infects and kills cancer cells but leaves the normal cells unharmed. Oncogenic viral therapy is important because of its ability to combine tumour-specific lysis and the delivery features of other anti-cancer drugs. Moreover, oncolytic virotherapy can protect normal tissues from exposure to therapeutic doses of chemotherapy or radiotherapy if combined with them in the therapeutic process [20]. Oncolytic virotherapy is also a form of immunotherapy by stimulating anti-tumour immune responses [12]. This type of alternative treatment may be more beneficial, especially in cases of incurable cancerous tumours, such as brain tumours and gliomas, that are not sufficiently eliminated by traditional and standard treatments [8, 26]. However, oncolytic viral therapy is still at its conceptual stages, and its full success in controlling cancer cells remains difficult to achieve. This includes the sensitivity of oncolytic viral therapy to tumours, which requires further research and extensive study. Virotherapy, like other anti-cancer therapies, must be examined for efficacy before it is applied to actual patients. Laboratory experiments need powerful tools such as mathematical models to help analyse experimental data and provide an archival base of experience for the development of subsequent experiments. The mechanistic underpinnings of complex and non-linear systems can be evaluated using the language of mathematics as well as predicting long-range behaviour. Using of mathematical models contributes to determining the appropriate parameters and simulating experiments to guide prediction for solving biological problems in real life [4]. We particularly investigate strategies aimed at optimizing the effectiveness of viral therapy by identifying the parameters that yield the most favorable treatment outcomes. Furthermore, we inquire about the conditions under which the best treatment outcomes are achievable. Various mathematical models have been created and examined to describe the behavior of virus dynamics, including the cited references [5, 14, 18, 23, 25].

One of the earliest attempts to formulate an essential ODE cancer virotherapy model was presented by Wordaz [34]. This work concluded that the virus and tumour might spread together despite intense viral lysis within cancer cells. This supports the necessity of choosing accurate techniques to evaluate the viral lysis process more successfully. Wordaz [34] emphasized that using a large number of infections to make the virus appear more efficient could be the least efficient at eliminating cancer in vivo. Since then, many expansions and additions have been made to consider virotherapy for many different cancer types, for example, hepatocellular carcinoma [3], cholangiocarcinoma [35], haemangioma [24], and glioma [27]. As one of many discoveries and hypotheses, many mathematical studies have shown that the size of the tumour can be reduced or even completely eliminated from the body's tissues, provided that the size of the viral explosion inside the tumour is huge [31]. One of the major questions associated with oncolytic virotherapy relates to understanding the role played by the tumour microenvironment during the virotherapy phase [6]. The occurrence of viral lysis is contingent upon the virus effectively infecting the host, preventing clearance by the immune system. It is known that oncolytic virus particles help activate immune cells in the tumour environment, and this is the focus of many researchers. However, we believe it is crucial to intensify the study of oncolytic virus dynamics within the tumour microenvironment to understand the consequences of tumour death in the absence of immune system involvement. The purpose is to determine how well the oncolytic virus performs its lethal function without being subjected to immune clearance.

Jenner et al. [13] introduced a significant mathematical model detailing the interaction between virus

particles and cancer cells. This model is designed to target and destroy cancerous tissue directly, bypassing the immune system's involvement. To gauge the importance of the effectiveness of oncolytic viral therapy, the researchers performed a local stability as well as bifurcation analysis with regard to this model. The results indicate that if the tumour grows weakly, even with viral decay, viral treatment can succeed in eliminating cancer cells in a large percentage. However, if the tumour percentage grows and the viral lysis process succeeds, the behaviour of the model shows more fluctuations between losing stability and maintaining it. The model shows that higher rates of tumour proliferation bring with them longer periods of oscillations and decay in the amplitude of uninfected cancer cells. The scientists determined that solely using oncolytic viruses would not suffice to fully eradicate the tumour. The model was derived in ordinary differential equations with integer order involving three classes: an uninfected cancer cells class $U(t)$, an infected cancer cells class $I(t)$ as well as a free virus particles class $V(t)$, where t represents time in days while r is the replicate rate of uninfected tumour cells. The rate of viral infection occurs at a constant rate within cancer cells and is denoted by β. After successful infection, the lysis process begins, followed by the explosion of infected tumour cells in the rate δ. New free viral particles are released at a rate of b to spread to neighbouring cancer cells. γ indicates the rate of decay of free virus particles. The governing model is given as follows:

$$\frac{dU}{dt} = rU - \beta UV, \quad \frac{dI}{dt} = \beta UV - \delta I, \quad \frac{dV}{dt} = b\delta I - \gamma V.$$

Biologically, unlimited exponential tumour growth cannot be realistically achieved due to nutrient and space limitations. Therefore, the inclusion of exponential growth in the model may be inappropriate for tumour growth under oncolytic virus treatment. At the same time, logistic growth operates under the premise that the expansion rate of a cancer cell population is directly related to the availability of space and internal resources necessary for its proliferation. As a population grows, the number of resources available for its growth decreases, resulting in a lower growth rate. Eventually, the growth rate of zero is obtained, while the population reaches its maximum size, known as carrying capacity [21]. For this reason, we will replace exponential growth with logistic growth in our research. The considered virotherapy cancer treatment is formulated as:

$$\frac{dU}{dt} = rU\left(1 - \frac{U+I}{k}\right) - \beta UV, \quad \frac{dI}{dt} = \beta UV - \delta I, \quad \frac{dV}{dt} = b\delta I - \gamma V, \tag{1.1}$$

where k is the carrying capacity for both types of tumour cells. However, Jenner's model with integer differential order misses the memory property, which is abundant in biological dynamics. To avoid this deficit, fractional order modelling is most appropriate to describe memory characteristics that are found in most biological phenomena [29]. Biological systems, recognized as complex adaptive entities, are heavily dependent on memory functions. With advancing research, a growing body of experts and academics notes that the principles of fractional-order theory align closely with real-world biology, providing a more precise depiction of the memory attributes of biological factors. Therefore, accounting for memory is vital for researchers investigating virus behavior for treatment purposes. In differential models based on fractional order, the subsequent state is influenced by the current state as well as all preceding states, a characteristic absent in integer order-based models [1]. Nevertheless, many differential equations, including fractional ones, are challenging to solve, necessitating more effective tools for implementing as well as simulating fractional-order viral therapy models, particularly in discrete forms. Occasionally, discretizing the continuous-time virotherapy model becomes necessary to accurately evaluate the impact of varying time steps on model behavior. In biological phenomena problems (especially those describing diseases and treatments), data collection is often discontinuous, so discrete-time models are more appropriate [7]. Building upon the insights mentioned earlier, we modify model (1.1) in this study by incorporating a discrete-time model that derives from a system of fractional order. This modification introduces two additional parameters to the new model: the parameter related to the memory effect "fractional-order" as well as the step size time parameter.

The remainder of the document is structured in the following manner. In Section 2, some preliminaries about the model are given. The fractional-order oncolytic virotherapy model with discrete time is derived in Section 3. The local stability analysis is presented in Section 4. The analysis of bifurcation is discussed in Section 5, while numerical simulations are performed in Section 6. To conclude, Section 7 offers a concise overview and discussion.

2. Equilibria

To reduce the parameters in the model (1.1) we set $\widetilde{t} = \delta t, U = k\widetilde{U}, I = k\widetilde{I}, V = k\widetilde{V}$. Now, the non-dimensionalized model of (1.1) may be expressed as:

$$\frac{d\widetilde{U}}{d\widetilde{t}} = \frac{r}{\delta}\widetilde{U}(1 - \widetilde{U} - \widetilde{I}) - \frac{k\beta}{\delta}\widetilde{U}\widetilde{V}, \quad \frac{d\widetilde{I}}{d\widetilde{t}} = \frac{k\beta}{\delta}\widetilde{U}\widetilde{V} - \widetilde{I}, \quad \frac{d\widetilde{V}}{d\widetilde{t}} = b\widetilde{I} - \frac{\gamma}{\delta}\widetilde{V}. \tag{2.1}$$

Taking $a = \frac{r}{\delta}, c = \frac{\beta k}{\delta}, d = \frac{\gamma}{\delta}$ and to avoid complexity, we set $\widetilde{t}, \widetilde{U}, \widetilde{I}, \widetilde{V}$ as t, U, I, V, respectively. Then, model (2.1) becomes:

$$\frac{dU}{dt} = aU(1 - U - I) - cUV, \quad \frac{dI}{dt} = cUV - I, \quad \frac{dV}{dt} = bI - dV. \tag{2.2}$$

Solving system (2.2) yields three equilibrium points, known as the trivial point $E_0\,(0,0,0)$, the virus-free point $E_1\,(1,0,0)$, and the coexistence point $E_2\left(\frac{d}{bc}, \frac{d}{b}V^*, V^*\right)$, where $V^* = \frac{a(bc-d)}{c(ad+bc)}$. E_2 indicates the existence of competition between all tumour cells and viruses.

Van den Driessche and Watmough [30] introduced the concept of a crucial parameter in mathematical models that characterize the spread of viruses within a community, called the basic reproduction number and typically represented as $\mathcal{R}_0$. This threshold provides insights into the propagation of infection within a population. The fundamental reproduction ratio is described as the average number of subsequent infections caused by a primary case among tumour cell populations [30]. When $\mathcal{R}_0 < 1$, the free virus equilibrium point tends to be asymptotically stable, indicating that, on average, an infected tumour cell yields less infections compared to another during its infectious period. In such instances, the infection cannot persist in the population of tumour cells. Conversely, when $\mathcal{R}_0$ exceeds 1, the equilibrium point for virus presence without any external interventions becomes unstable, initiating an infection outbreak among the tumour cells. The fundamental reproductive number, $\mathcal{R}_0$, serves as an indicator of the capacity of the virus to propagate within the tumour cell population. To determine the $\mathcal{R}_0$, model (2.2) may be expressed as:

$$\frac{d\mathbf{T}(t)}{dt} = \mathbf{W}(T) - \mathbf{N}(T),$$

where $\mathbf{T}(t) = \begin{pmatrix} U(t) \\ I(t) \\ V(t) \end{pmatrix}, \mathbf{W}(T) = \begin{pmatrix} 0 \\ cU(t)V(t) \\ 0 \end{pmatrix}$, and

$$\mathbf{N}(T) = \begin{pmatrix} -aU(t)[1 - U(t) - I(t)] + cU(t)V(t) \\ I(t) \\ -bI(t) + dV(t) \end{pmatrix}.$$

We now define K and L as the Jacobian matrix of $\mathbf{W}$ and $\mathbf{N}$ at E_1, respectively. Then, we obtain:

$$KL^{-1} = \begin{pmatrix} 0 & 0 & 0 \\ 0 & \frac{cb}{d} & \frac{c}{d} \\ 0 & 0 & 0 \end{pmatrix}.$$

KL^{-1} is said to be the next-generation matrix. According to [30], $\mathcal{R}_0$ is expressed as the spectral radius of KL^{-1}, which gives $\mathcal{R}_0 = \frac{bc}{d}$.

Lemma 2.1. *Should $\mathcal{R}_0 = 1$, model (2.2) possesses solely a free-virus equilibrium point. Conversely, should $\mathcal{R}_0 > 1$, model (2.2) is characterised by a tumour-infected equilibrium point.*

Proof. If there exists a tumour infected equilibrium of (2.2), then E_2 must satisfy the following equations:

$$\begin{cases} aU^*(1 - U^* - I^*) - cU^*V^* = 0, \\ cU^*V^* - I^* = 0, \\ bI^* - dV^* = 0. \end{cases} \tag{2.3}$$

It is assumed that there is a unique coexistence solution to (2.3), which yields

$$\begin{cases} U^* = \frac{1}{\mathcal{R}_0}, \\ I^* = \frac{d}{b}V^*, \\ V^* = \frac{a(\mathcal{R}_0 - 1)}{c(\mathcal{R}_0 + a)}. \end{cases}$$

It is clear that U^* is consistently positive. However, both I^* and V^* are positive solely when $\mathcal{R}_0 > 1$. □

3. Fractional-order mathematical model and its discretization

This section is devoted to deriving the fractional-order model from its integer-order counterpart. An approximation scheme will be applied to the fractional order model to construct a new discrete-time oncolytic virotherapy model with fractional order.

3.1. Fractional order model

Fractional calculus has attracted the attention of many researchers in the field of mathematical modelling over the past few decades. It is a more suitable tool to describe natural phenomena that have memory and hereditary properties, such as cancer diseases. Differential equations with fractional order are closely connected with memory for cancer disease models [11]. Most cancer disease models have been described by using differential equations with integer order to understand their behaviours. The behaviours of these models lack the effect of memory characteristics, which is already well-captured by fractional order differential equations [37]. Long-term memory is an important property in the models that describe cancer disease problems. Fractional-order models showed greater accuracy in the retention of memory characteristics, un-locality, and spatial heterogeneity [2]. Several definitions of fractional derivatives have been introduced in the literature [28, 37]. Caputo's definition [2] is still the most frequently used in literature till now. Caputo definition of fractional derivatives is as follows below.

Definition 3.1 ([2]). The fractional integral of order $\beta \in \mathbb{R}^+$ of the function $f(t)$, $t > 0$, is defined by $I^\beta f(t) = \int_0^t \frac{(t-s)^{\beta-1}}{\Gamma(\beta)} f(s)\, ds$. Meanwhile, the fractional derivative of order $\alpha \in (n-1, n)$ of $f(t)$, $t > 0$, is expressed by $D^\alpha f(t) = I^{n-\alpha} D^n f(t)$, $\alpha > 0$, in which $f^{(n)}$ denotes the n-order derivative of $f(t)$, $n = [\alpha]$ resembles the α value rounded up to the nearest integer, I^β denotes the β-order Riemann-Liouville integer operator, while $\Gamma(.)$ refers to the Euler's Gamma function. The operator D^α is known as the "α-order Caputo differential operator".

Under specific conditions, Caputo's definition of the fractional derivative may be more suitable and convenient for the function $f(t)$ compared to the Riemann-Liouville fractional derivative. This is particularly true when taking into consideration initial conditions of $f(t)$ as α comes closer to n. Hence, the fractional-order model (2.2) formulation may be written as:

$$D^\alpha U(t) = aU(1 - U - I) - cUV, \quad D^\alpha I(t) = cUV - I, \quad D^\alpha V(t) = bI - dV, \tag{3.1}$$

where $t > 0, D^\alpha = \frac{d^\alpha}{dt^\alpha}$ is in the sense the Caputo derivative, while α refers to the fractional-order satisfying $0 < \alpha \leqslant 1$.

3.2. Existence and uniqueness of the solution

The theorem presented below provides the necessary conditions to ensure both the existence as well as the uniqueness of the solution for model (3.1).

Theorem 3.2. *A sufficient condition for the solution of model* (3.1) *to be both existent and unique within the domain* $\Phi \times (0, T]$ *given the initial conditions* $X(0) = X_0$ *and for* $t \in (0, T]$ *is:*

$$C = \frac{T^n}{\Gamma(1+n)} \max\{[a(1+3\epsilon)+2c\epsilon], [b+a\epsilon+1], d\} < 1$$

for some $\delta \in \mathbb{R}^+$.

Proof. The fractional-order model (3.1) may be expressed as

$$D_t^\alpha X(t) = F(X(t)), \ t \in (0, T], \ X(0) = X_0, \ X = \begin{bmatrix} U \\ I \\ V \end{bmatrix}, \ X_0 = \begin{bmatrix} U_0 \\ I_0 \\ V_0 \end{bmatrix}, \ F(X) = \begin{bmatrix} aU(1-U-I)-cUV \\ cUV-I \\ bI-dV \end{bmatrix}.$$

Let $\|P\| = \sup_{t \in (0,T]} |P(t)|$. Then, the norm of the matrix $G = [g_{ij}[t]]$ is defined by

$$\|G\| = \max_i \sum_j g_{ij}[t]. \tag{$*$}$$

We investigate the existence as well as uniqueness of the solution within the domain $\Phi \times (0, T]$, focusing on

$$\Phi = \{(U, I, V) : \max(|U|, |I|, |V|) \leqslant \epsilon\}.$$

Hence, the solution of model (3.1) is given as follows

$$X = X_0 + \frac{1}{\Gamma(\alpha)} \int_0^t (t-\tau)^{\alpha-1} F(X(\tau)) d\tau = Q(X).$$

Hence,

$$Q(X_1) - Q(X_2) = \frac{1}{\Gamma(\alpha)} \int_0^t (t-\tau)^{\alpha-1} [F(X_1(\tau)) - F(X_2(\tau))] d\tau.$$

Therefore, we attain the following inequality

$$|Q(X_1) - Q(X_2)| \leqslant \frac{1}{\Gamma(\alpha)} \int_0^t \left|(t-\tau)^{\alpha-1} [F(X_1(\tau)) - F(X_2(\tau))]\right| d\tau,$$

$$\leqslant \frac{1}{\Gamma(\alpha)} \int_0^t \left|(t-\tau)^{\alpha-1}\right| |F(X_1(\tau)) - F(X_2(\tau))| d\tau.$$

Using the intermediate value theorem, we have

$$|Q(X_1) - Q(X_2)| = \nabla Q \|X_1 - X_2\|,$$

where ∇F is the matrix norm of the Jacobian matrix of the model (3.1). Now we arrive at

$$\nabla F = \max\{[a(1-2U-I)-2cV], [b-aU-1], [-d]\}.$$

Using Eq. ($*$), we get

$$\nabla F < \max\{[a(1+3\epsilon)+2c\epsilon], [b+a\epsilon+1], d\}.$$

Then,

$$\|Q(X_1) - Q(X_2)\| \leqslant \frac{T^n}{\Gamma(1+n)} \max\{[a(1+3\delta)+2c\delta], [b+a\delta+1], d\} \|X_1 - X_2\| \leqslant C \|X_1 - X_2\|,$$

where

$$C = \frac{T^n}{\Gamma(1+n)} \max\{[a(1+3\epsilon)+2c\epsilon], [b+a\epsilon+1], d\}.$$

If $C < 1$, it follows that the mapping $X = Q(X)$ is a contraction mapping. $\qquad\square$

3.3. Discrete-time model with fractional order

In general, mathematical cancer models use multi-scale approaches, combining continuous modelling using differential equations and discrete modelling using different equations. Continuous modelling often describes the dynamics of extracellular environmental factors. In contrast, discrete modelling is designed to describe cancer cell migration and the progression of metastasis based on a set of scientific hypotheses. At discrete time steps, new non-overlapping generations of population cells are produced, observing scientific rules that arise on the state of the current cell and its neighbouring cells. Patient information is gathered at specific intervals and at discrete times, making discrete-time models potentially more suitable for analysis and application. In this subsection, a new discrete-time model based on fractional-order the oncolytic virotherapy model (3.1) is presented. Elsayed et al. [10] introduced a proper approximation method to formulate a discrete-time model from a fractional-order model. For any $n \geqslant 0$, let $U_n = U(n)$, $I_n = I(n)$, and $V_n = V(n)$. Now, by applying the approximation method in [10], the model (3.1) may be discretized as follows:

$$
\begin{aligned}
U_{n+1}(t) &= U_n + \frac{s^\alpha}{\Gamma(1+\alpha)} \left[aU_n(1 - U_n - I_n) - cU_nV_n \right], \\
I_{n+1}(t) &= I_n + \frac{s^\alpha}{\Gamma(1+\alpha)} \left[cU_nV_n - I_n \right], \\
V_{n+1}(t) &= V_n + \frac{s^\alpha}{\Gamma(1+\alpha)} \left[bI_n - dV_n \right],
\end{aligned}
\tag{3.2}
$$

where the time step size parameter s is greater than 0 and initial conditions $U_0 > 0$, $I_0 > 0$, and $V_0 > 0$. Model (3.2) includes two additional and influential parameters, which are not included in the original model, known as the fractional order parameter α as well as the time step size s. With these two new parameters, our new model (3.2) is expected to introduce new and complex dynamic behaviours.

4. Stability analysis

In this segment, we examine the equilibrium stability analysis within the model (3.2). Let us consider the specified non-linear discrete-time system:

$$
x_{k+1} = f_\mu(x_k),
\tag{4.1}
$$

where $x_{k+1}, x_k \in \mathbb{R}^n$ denote the state vectors, k refers to the iterative index, f_μ denotes the non-linear function vector while $\mu \in \mathbb{R}^m$ refers to the parameter-independent vector. Here, let the characteristic polynomial of (4.1) at the fixed point x_0 be:

$$
F_\mu(\lambda) = a_0\lambda^n + a_1\lambda^{n-1} + \cdots + a_{n-1}\lambda + a_n = 0,
$$

in which $a_i = a_i(\mu)$, $i = 0,\ldots,n$ while $a_0 = 1$. The fixed point x_0 is asymptotically stable provided that all eigenvalues λ_i of Jacobian matrix $J(\mu_0, x_0)$ of model (4.1) lie in the unit circle. Otherwise, x_0 is unstable. The statement of the following lemma is necessary.

Lemma 4.1 ([16]). *A discrete non-linear dynamical system is considered with a fixed point x_0 as well as the associated Jacobian matrix $J(\mu_0, x_0)$ has n eigenvalues λ_i ($i = 1, 2, \ldots, n$). Then*

(i) *x_0 is locally asymptotic stable if $|\lambda_i| < 1$;*
(ii) *x_0 is unstable (source) if $|\lambda_i| > 1$;*
(iii) *x_0 is unstable (saddle) if at least one $|\lambda_i| > 1$ ($i \in K_1 \subset \{1, 2, \ldots, n\}$) and the other $|\lambda_j| < 1$ ($j \in K_2 \subset \{1, 2, \ldots, n\}$) with $K_1 \cup K_2 = \{1, 2, \ldots, n\}$ as well as $K_1 \cap K_2 = \phi$;*
(iv) *x_0 is a non-hyperbolic point if only one of $|\lambda_i| = 1$.*

Theorem 4.2. *The equilibrium point E_0 refers to a saddle point when $s < \min\left\{\sqrt[\alpha]{2\Gamma(1+\alpha)}, \sqrt[\alpha]{\frac{2\Gamma(1+\alpha)}{d}}\right\}$ and unstable (source), when $s > \max\left\{\sqrt[\alpha]{2\Gamma(1+\alpha)}, \sqrt[\alpha]{\frac{2\Gamma(1+\alpha)}{d}}\right\}$.*

Proof. To study the stability analysis of E_0, the Jacobian matrix at E_0 is given as

$$J(E_0) = \begin{bmatrix} 1 + \frac{s^\alpha}{\Gamma(1+\alpha)}(a) & 0 & 0 \\ 0 & 1 - \frac{s^\alpha}{\Gamma(1+\alpha)} & 0 \\ 0 & \frac{s^\alpha}{\Gamma(1+\alpha)}(b) & 1 - \frac{s^\alpha}{\Gamma(1+\alpha)}(d) \end{bmatrix}.$$

The eigenvalues accompanying $J(E_0)$ are $\lambda_1 = 1 + \frac{s^\alpha}{\Gamma(1+\alpha)}(a)$, $\lambda_2 = 1 - \frac{s^\alpha}{\Gamma(1+\alpha)}$, and $\lambda_3 = 1 - \frac{s^\alpha}{\Gamma(1+\alpha)}(d)$. λ_1 is always greater than 1. It is clear that $|\lambda_{2,3}| < 1$ if $s < \min\left\{\sqrt[\alpha]{2\Gamma(1+\alpha)}, \sqrt[\alpha]{\frac{2\Gamma(1+\alpha)}{d}}\right\}$, while $|\lambda_{2,3}| > 1$ if $s > \max\left\{\sqrt[\alpha]{2\Gamma(1+\alpha)}, \sqrt[\alpha]{\frac{2\Gamma(1+\alpha)}{d}}\right\}$. According to Lemma 4.1, E_0 is a saddle point if $s < \min\left\{\sqrt[\alpha]{2\Gamma(1+\alpha)}, \sqrt[\alpha]{\frac{2\Gamma(1+\alpha)}{d}}\right\}$ and unstable (source) if $s > \max\left\{\sqrt[\alpha]{2\Gamma(1+\alpha)}, \sqrt[\alpha]{\frac{2\Gamma(1+\alpha)}{d}}\right\}$. □

Theorem 4.3. *When $\mathcal{R}_0 \leqslant 1$, then E_1 has the following properties:*

(i) E_1 *is asymptotically stable and called (sink) when* $s < s_1 = \min\left\{\sqrt[\alpha]{\frac{2\Gamma(1+\alpha)}{a}}, \sqrt[\alpha]{\frac{4\Gamma(1+\alpha)}{1+d-\sqrt{\Delta}}}, \sqrt[\alpha]{\frac{4\Gamma(1+\alpha)}{1+d+\sqrt{\Delta}}}\right\}$;

(ii) E_1 *is unstable (source) when* $s > s_2 = \max\left\{\sqrt[\alpha]{\frac{2\Gamma(1+\alpha)}{a}}, \sqrt[\alpha]{\frac{4\Gamma(1+\alpha)}{1+d-\sqrt{\Delta}}}, \sqrt[\alpha]{\frac{4\Gamma(1+\alpha)}{1+d+\sqrt{\Delta}}}\right\}$;

(iii) E_1 *is unstable (saddle) when* $s_1 < s < s_2$;

(iv) E_1 *is non-hyperbolic when* $s = \sqrt[\alpha]{\frac{2\Gamma(1+\alpha)}{a}}$ *or* $s = \sqrt[\alpha]{\frac{4\Gamma(1+\alpha)}{1+d-\sqrt{\Delta}}}$ *or* $s = \sqrt[\alpha]{\frac{4\Gamma(1+\alpha)}{1+d+\sqrt{\Delta}}}$*, where* $\Delta = (d-1)^2 + 4bc$.

Proof. The Jacobian matrix at E_1 has the form:

$$J(E_1) = \begin{bmatrix} 1 - \frac{s^\alpha}{\Gamma(1+\alpha)}(a) & -\frac{s^\alpha}{\Gamma(1+\alpha)}(a) & -\frac{s^\alpha}{\Gamma(1+\alpha)}(c) \\ 0 & 1 - \frac{s^\alpha}{\Gamma(1+\alpha)} & \frac{s^\alpha}{\Gamma(1+\alpha)}(c) \\ 0 & \frac{s^\alpha}{\Gamma(1+\alpha)}(b) & 1 - \frac{s^\alpha}{\Gamma(1+\alpha)}(d) \end{bmatrix}.$$

The corresponding eigenvalues of $J(E_1)$ are $\lambda_1 = 1 - \frac{s^\alpha}{\Gamma(1+\alpha)}(a), \lambda_{2,3} = 1 - \frac{s^\alpha}{2\Gamma(1+\alpha)}\left[1 + d \pm \sqrt{\Delta}\right]$, where $\Delta = (d-1)^2 + 4bc > 0$. It is easy to deduce that if $\mathcal{R}_0 \leqslant 1$, then $1 + d - \sqrt{\Delta} > 0$. Hence, $\lambda_{2,3}$ cannot be greater than 1. Thus, by applying Lemma 4.1, the findings (i)-(iv) may be accomplished. □

Now, we investigate the stability with regards to the tumour-infected equilibrium point E_2. To determine the stability conditions of E_2, Schur-Cohn [15] put in an alternative criterion when $n \geqslant 3$ using the following theorem.

Theorem 4.4 ([15])**.** *The characteristic equation $F(\lambda)$ has all its roots inside the unit circle if and only if*

(a) $F(1) > 0$ *and* $(-1)^n F(-1) > 0$;

(b) $\Delta_1^\pm > 0, \Delta_3^\pm > 0, \ldots, \Delta_{n-3}^\pm > 0, \Delta_{n-1}^\pm > 0$ *(when n is even), or* $\Delta_2^\pm > 0, \Delta_4^\pm > 0, \ldots, \Delta_{n-3}^\pm > 0, \Delta_{n-1}^\pm > 0$ *(when n is odd).*

Meanwhile, the determinant of the sequences is:

$$\Delta_i(\mu, x) = \left| \begin{pmatrix} 1 & a_1 & a_2 & \cdots & a_{i-1} \\ 0 & 1 & a_1 & \cdots & a_{i-2} \\ 0 & 0 & 1 & \cdots & a_{i-3} \\ \vdots & \vdots & \vdots & \vdots & \vdots \\ 0 & 0 & 0 & \cdots & 1 \end{pmatrix} \pm \begin{pmatrix} a_{n-i+1} & a_{n-i+2} & \cdots & a_{n-1} & a_n \\ a_{n-i+2} & a_{n-i+3} & \cdots & a_n & 0 \\ \vdots & \vdots & \vdots & \vdots & \vdots \\ a_{n-1} & a_n & \cdots & 0 & 0 \\ a_n & 0 & \cdots & 0 & 0 \end{pmatrix} \right|,$$

for $i = 1, \ldots, n$. The stability conditions concerning $E_2(U^*, I^*, V^*)$ can be examined by computing the Jacobian matrix at E_2 as follows:

$$J(E_2) = \begin{bmatrix} 1 + \frac{s^\alpha}{\Gamma(1+\alpha)}\left(\frac{a}{\mathcal{R}_0}\right) & -\frac{s^\alpha}{\Gamma(1+\alpha)}\left(\frac{a}{\mathcal{R}_0}\right) & -\frac{s^\alpha}{\Gamma(1+\alpha)}\left(\frac{c}{\mathcal{R}_0}\right) \\ \frac{s^\alpha}{\Gamma(1+\alpha)}\left[\frac{a(\mathcal{R}_0-1)}{\mathcal{R}_0+a}\right] & 1 - \frac{s^\alpha}{\Gamma(1+\alpha)} & \frac{s^\alpha}{\Gamma(1+\alpha)}\left(\frac{c}{\mathcal{R}_0}\right) \\ 0 & \frac{s^\alpha}{\Gamma(1+\alpha)}(b) & 1 - \frac{s^\alpha}{\Gamma(1+\alpha)}(d) \end{bmatrix}. \tag{4.2}$$

The equation that defines the characteristics associated with the Jacobian matrix at E_2 can be expressed in the following manner:

$$P(\lambda) = a_0\lambda^3 + a_1\lambda^2 + a_2\lambda + a_3 = 0. \tag{4.3}$$

Consider that we have:

$$l_1 = \frac{cb(d+1) + ad}{cb}, \quad l_2 = \frac{ad\left[cb(d+a+1) + ad^2\right]}{cb(ad+cb)}, \quad l_3 = \frac{ad^2}{cb}(\mathcal{R}_0 - 1), \quad h(s,\alpha) = \frac{s^\alpha}{\Gamma(1+\alpha)}.$$

Then, the coefficients of the characteristic equation (4.3) can be written as:

$$a_0 = 1, \quad a_1 = l_1 h - 3, \quad a_2 = l_2 h^2 - 2l_1 h + 3, \quad a_3 = l_3 h^3 - l_2 h^2 + l_1 h - 1.$$

Applying Theorem 4.4, all roots of equation (4.3) are located within the unit circle when the following conditions are met:

$$\begin{cases} F(1) \equiv 1 + a_1 + a_2 + a_3 > 0, \\ (-1)F(-1) \equiv 1 - a_1 + a_2 - a_3 > 0, \\ \Delta_2^+ \equiv 1 + a_2 - a_1 a_3 - a_3^2 > 0, \\ \Delta_2^- \equiv 1 - a_2 + a_1 a_3 - a_3^2 > 0, \end{cases}$$

which leads to

$$\begin{cases} l_3 h^3 > 0, \\ -l_3 h^3 + 2l_2 h^2 - 4l_1 h + 8 > 0, \\ -h(l_3^2 h^5 - 2l_2 l_3 h^4 + (3l_1 l_3 + l_2^2)h^3 + (-3l_1 l_2 - 5l_3)h^2 + (2l_1^2 + 4l_2)h - 4l_1) > 0, \\ -h^3(l_3^2 h^3 - 2l_2 l_3 h^2 + (l_1 l_3 + l_2^2)h - l_1 l_2 + l_3) > 0. \end{cases} \tag{4.4}$$

Depending on Theorem 4.4, E_2 is asymptotically stable if h has at least one solution that satisfies (4.4). Otherwise, E_2 is unstable. We can clearly observe that the stability regions of the E_2 equilibrium point may be expressed in parameter space utilising the inequality conditions outlined in (4.4). These conditions depend on various parameters, including the fractional-order parameter and step size of the system (3.2). We illustrate these regions for different parameter scenarios to examine the effective parameters by investigating possible bifurcation types in our fractional-order oncolytic virotherapy model with discrete time, as deduced in the numerical simulations section.

5. Bifurcations

Bifurcation, signifying a qualitative shift in dynamical characteristics, represents a critical phenomenon associated with the destabilization of a system. In the dynamics of virotherapy, numerous parameters exist, each carrying its own significance, affecting the whole model. Therefore, our purpose in this section is to highlight these effects by using bifurcation analysis for some important parameters in the model (3.2). The parameters are examined to understand the possible outcomes of the treatment as each of them changes, including the fractional-order parameter, which relates to the memory effect α, step size time s, the infection rate β, and the virus spread rate b. We explore various common bifurcation types in discretized fractional-order models, including codimension-one and codimension-two bifurcations of model (3.2). The fundamental idea of detecting bifurcations is centred on calculating the eigenvalues of

the Jacobian matrix at each essential bifurcation point throughout the parameter space. Nevertheless, the task of evaluating eigenvalues one by one across the parameter space in complex, high-dimensional dynamical systems can prove to be quite laborious. Thus, to accelerate the process of identifying stability conditions within systems involving multiple parameters, it is possible to establish an explicit critical criterion without requiring eigenvalue calculations, thus providing substantial computational simplification [32]. In our study of bifurcation conditions, we concentrate on the characteristic equations' coefficients instead of the functions of the eigenvalues of the Jacobian matrix [15, 22, 32, 33, 36].

5.1. Codimension one bifurcations

In the codim-1 bifurcation section, we explore the concept of bifurcation within the discretised fractional-order virotherapy model (3.2). Through the use of bifurcation diagrams, we can offer insightful visual representations of how our system dynamics alter with modifications in its parameters. Algebraic methods are employed to construct the existing conditions for the codim-1 N-S, flip as well as fold bifurcations of the model (3.2).

5.1.1. Neimark-Sacker bifurcation

In the realm of non-linear discrete-time systems, the Neimark-Sacker bifurcation mirrors the Hopf bifurcation seen in continuous-time systems. The Neimark-Sacker bifurcation is characterized by the matrix $J(\mu_0, \mathbf{x}_0)$ possessing a set of complex conjugate eigenvalues that are situated on the unit circle. In contrast, all other eigenvalues are located within the unit circle. Considering the potential for a Neimark-Sacker bifurcation at $x = x_0$ when $\mu = \mu_0$, it is important to revisit the related theorem.

Theorem 5.1 ([32]). *For a general system of n dimensions as described by equation* (4.1)*, it experiences a loss of stability through a Neimark-Sacker bifurcation when the bifurcation parameter is set to $\mu = \mu_0$, but only if the specified conditions are satisfied:*

(C_{11}) *eigenvalue assignment:* $\Delta_{n-1}^-(\mu_0) = 0, (-1)^n F_{\mu_0}(-1) > 0, F_{\mu_0}(1) > 0, \Delta_{n-1}^+(\mu_0) > 0, \Delta_j^\pm(\mu_0) > 0, j = n-3, n-5, \ldots, 1$ *(or 2) when n is even (or odd, respectively);*

(C_{12}) *transversality condition:* $\dfrac{d\Delta_{n-1}^-(\mu)}{d\mu} \neq 0$;

(C_{13}) *nonresonance condition:* $\cos\left(\frac{2\pi}{m}\right) \neq 1 - \dfrac{F_{\mu_0}(1)\Delta_{n-3}^-(\mu_0)}{2\Delta_{n-2}^+(\mu_0)}$, *where $m = 3, 4, 5, \ldots$.*

The condition denoted by (C_{11}) indicates the presence of a conjugate complex eigenvalue pair situated on the unit circle, while any additional eigenvalues, should they exist, are positioned within the unit circle. On the other hand, the condition (C_{12}) means that the conjugate complex eigenvalues should pass through the unit circle with non-zero speed. Meanwhile, the condition (C_{13}) points to that $\lambda_1^l(\mu_0, \mathbf{x}_0) \neq 1, l = 3, 4, \ldots$. Let us consider the following:

$$\Delta_2^- \equiv \xi_1 = m_2 - m_1 - 2 - \left(m_3 + \tfrac{1}{2}m_2 - m_1 - 1\right)(m_3 - m_1 + 2),$$
$$\Delta_2^+ \equiv \xi_2 = -m_2 + m_1 + 4 - \left(m_3 + \tfrac{1}{2}m_2 - m_1 - 1\right)(m_3 + m_2 - m_1 - 4),$$
$$F(1) \equiv \xi_3 = m_3,$$
$$F(-1) \equiv \xi_4 = m_3 + 2m_2 - 2m_1 - 8,$$

where

$$m_1 = \frac{ad + 2b(d+1)h(s,\alpha)}{bh(s,\alpha)}, \quad m_2 = \frac{ad\beta(ad^2 + 2b(d+a+1)h(s,\alpha))}{bh(s,\alpha)(ad + 2bh(s,\alpha))}, \quad m_3 = \frac{ad\beta^2(2bh(s,\alpha) - d)}{2bh(s,\alpha)}.$$

Applying the above conditions (C_{11})-(C_{13}), we can obtain the existence conditions with regards to N-S bifurcation of model (3.2) as follows.

$$\begin{cases} \xi_1 = 0, \\ \xi_2 > 0, \\ \xi_3 > 0, \\ \xi_4 < 0, \\ \xi_5 \neq 0, \end{cases} \tag{5.1}$$

where

$$\begin{aligned} \xi_5 = {} & h(s,\alpha)^3(\ln(s) - \Psi(1+\alpha)) \left[-6 \left[\frac{ad(2b\beta - d)}{2b\beta} \right]^2 h(s,\alpha)^3 + 10 \left[\frac{ad(2b\beta - d)}{2b\beta} \right] \right. \\ & \times \left[\frac{ad(2b\beta(d+a+1) + ad^2)}{2b\beta(ad+2b\beta)} \right] h(s,\alpha)^2 - 4 \left[\frac{2b\beta(d+1) + ad}{2b\beta} \right] \left[\frac{ad(2b\beta - d)}{2b\beta} \right] h(s,\alpha) \\ & - 4l_2^2 h(s,\alpha) + 3 \left[\frac{2b\beta(d+1) + ad}{2b\beta} \right] \left[\frac{ad(2b\beta(d+a+1) + ad^2)}{2b\beta(ad+2b\beta)} \right] - 3 \left[\frac{ad(2b\beta - d)}{2b\beta} \right] \right]. \end{aligned}$$

    N-S bifurcation emerges if there is at least one real solution that satisfies the semi-algebraic system (5.1). Fig. 1 shows the area of solution of (5.1) when α is chosen as the N-S bifurcation parameter. The red line in Fig. 1 indicates the equation $\xi_1 = 0$. The green, blue, and black lines shown in Fig. 1 represent the inequalities $\xi_2 > 0$, $\xi_3 > 0$, and $\xi_4 > 0$, respectively. The shaded region represents the solution of these three inequalities. There is no real solution for the inequalities $\xi_2 > 0$, $\xi_3 > 0$, and $\xi_4 > 0$ into the blank region. We have to point out that the line representing the transversality condition in (5.1) doesn't appear inside the first quarter of the $\beta - \alpha$ plane. Theorem 5.1 establishes that an N-S bifurcation point, which is located on the red line within the shaded region shown in Fig. 1, fulfils the criteria specified in (5.1).
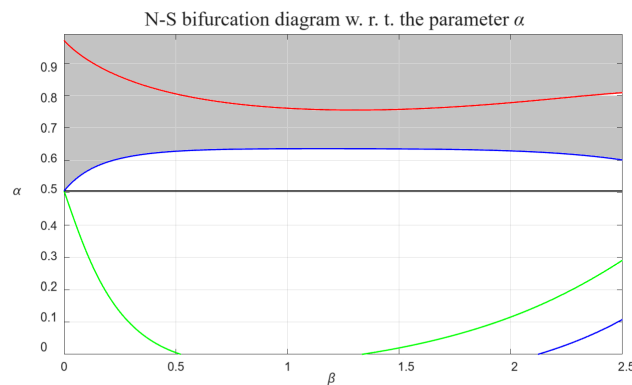

Figure 1: The conditions described in the semi-algebraic system (5.1) are exemplified for the values $r = 2, k = 1, \beta = 2, \delta = 0.5, b = 0.9, \gamma = 0.5, s = 1.8$, and $\alpha \in (0, 0.99)$.

5.1.2. Flip bifurcation

    A flip or period-doubling bifurcation occurs exclusively within a non-linear discrete-time system. At the point of the flip bifurcation, the system transitions into a new dynamical state, exhibiting a period that is double that of its original state. This sequence of period-doubling bifurcations has the potential to drive the system towards chaos. We express the Jacobian matrix $J(\mu_0, \mathbf{x}_0)$ of (4.2) at an equilibrium point x_0 and μ_0 is a bifurcation parameter. In this bifurcation, the Jacobian matrix $J(\mu_0, \mathbf{x}_0)$ possesses a singular eigenvalue that resides on the unit circle, being real and equivalent to -1, whilst the remainder are situated within the unit circle. [33] proposed the algebraic criterion conditions that determine the flip bifurcation to be occurring in a dynamical discrete-time system.

Proposition 5.2 ([2, 33]). *In a general n-dimensional framework as described by equation (4.1), a flip bifurcation occurs at $\mu = \mu_0$ if and only if the specified criteria are met:*

(C$_{21}$) *eigenvalue assignment:* $F_{\mu_0}(-1) = 0$, $F_{\mu_0}(1) > 0$, $\Delta_{n-1}^{\pm}(\mu_0) > 0$ *and* $\Delta_j^{\pm}(\mu_0) > 0$, $j = n-3, n-5, \ldots, 1$ *(or 2) when* n *is even (or odd, accordingly);*

(C$_{22}$) *transversality condition:* $\dfrac{\sum_{i=1}^{n} a_i'(-1)^{n-i}}{\sum_{t=1}^{n}(n-j+1)(-1)^{n-j}a_{j-1}} \neq 0$, *where* a_i' *refers to the derivative of* $a_i(\mu)$ *with respect to the bifurcation parameter* μ *at* $\mu = \mu_0$.

The condition (C$_{21}$) assures that one real eigenvalue $\lambda_1(\mu_0)$ of $J(\mu_0, \mathbf{x}_0)$ lies on the unit circle and equals to -1 while the others lie inside the unit circle. Moreover, the condition (C$_{22}$) says that $\lambda_1(\mu_0)$ should passes throughout the unit circle with non-zero speed. Applying Proposition 5.2, we conclude that the conditions of flip bifurcation of the model (3.2) are as follows. Based on the Proposition 5.2, the model (3.2) may undergo a flip bifurcation at E_2 with codimension of one bifurcation parameter of s or α if the following conditions are met:

$$\begin{cases} \xi_1 > 0, \\ \xi_2 > 0, \\ \xi_3 > 0, \\ \xi_4 = 0, \\ \xi_6 \neq 0, \\ \xi_7 \neq 0, \end{cases} \tag{5.2}$$

where

$$\xi_6 = \frac{adh(s,\alpha)}{2\beta^2 b(ad + 2b\beta)^2}\left[8\beta^2((h(s,\alpha) + \frac{h(s,\alpha)^2}{2})d + ah(s,\alpha) + h(s,\alpha) - 2)b^2 \right.$$
$$\left. + 4a\beta d(-4 + (h(s,\alpha)^2 + 2h(s,\alpha))d)b + a^2d^2(-4 + (h(s,\alpha)^2 + 2h(s,\alpha))d)\right],$$

$$\xi_7 = \frac{-adh(s,\alpha)(4\beta^2(ah(s,\alpha) + dh(s,\alpha) + h(s,\alpha) - 4)b^2 + 4ad\beta(dh(s,\alpha) - 4)b + a^2d^2(dh(s,\alpha) - 4))}{2\beta^2 b(ad + 2b\beta)^2}.$$

Flip bifurcation occurs if there is at least one real solution that satisfies the semi-algebraic system (5.2) when s is considered as a flip bifurcation parameter. Fig. 2 depicts the area of solution of (5.2). The shaded area shows the solution's area of the inequalities $\xi_2 > 0$, $\xi_3 > 0$, and $\xi_4 > 0$, which are surrounded by the green, black, and blue lines. The blank region is the area in which the inequalities $\xi_2 > 0$, $\xi_3 > 0$, and $\xi_4 > 0$ fail to get one real solution. The red line stands to the equation $\xi_1 = 0$, while the dotted yellow line denotes the transversality conditions $\xi_6 \neq 0$ and $\xi_7 \neq 0$ in (5.2). According to Proposition 5.2, there is a flip bifurcation point lying on the red line placed into the shaded area in Fig. 2 that can satisfy the conditions in (5.2).
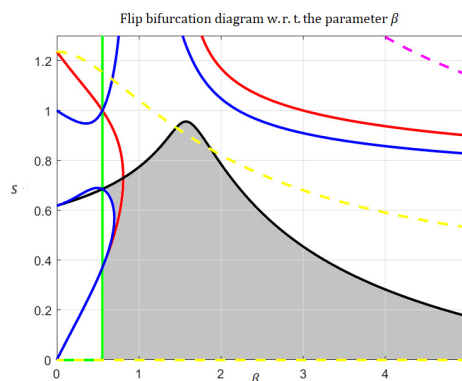

Flip bifurcation diagram w. r. t. the parameter β

Figure 2: The conditions described in the semi-algebraic system (5.2) are exemplified for the values $r = 2.7, k = 1, \delta = 0.5, b = 0.9, \gamma = 0.5, \alpha = 0.99, s = 1.3$, and $\beta \in (0.725, 0.9)$.

A stationary bifurcation (also called a fold bifurcation) can occur if the Jacobian matrix $J(\mu_0, x_0)$ of (4.2) has a single real eigenvalue equal to 1 [15]. This bifurcation may be one of saddle-node, transcritical,

or pitchfork bifurcation. In order to avoid redundancy, the fold bifurcation conditions can be obtained by replacing $F_{\mu_0}(-1) = 0, F_{\mu_0}(1) > 0$ in the condition (C_{21}) above by $(-1)^n F_{\mu_0}(-1) > 0, F_{\mu_0}(1) = 0$ [15]. In the numerical simulation section, we will provide a comprehensive graphical exposition of the fold bifurcation that transpired due to variations in the burst size rate parameter of the virus, specifically in case 3. Nevertheless, identifying the exact kind of fold bifurcation within a system requires additional examination.

5.2. Codimension-two bifurcations

This section focuses on examining the overlap between flip and N-s bifurcations within model (3.2), specifically addressing the phenomenon known as codimension-two flip-N-S bifurcations. The codimension-two bifurcation in non-linear dynamical systems, known as "double crises", relies on continuing two critical parameters of bifurcation.

5.2.1. Flip-N-S bifurcation

The Flip-Neimark-Sacker bifurcation represents a codimension-two singularity within discrete-time system bifurcations. The essential conditions for the emergence of a flip-N-S bifurcation are detailed in the theorem provided.

Theorem 5.3 ([22, 36]). *For a general n-dimensional system* (4.1)*, its stability is compromised through a flip-N-S bifurcation when* $\mu = \mu_0$ *if and only if the subsequent criteria are met:*

(C_{31}) *eigenvalue assignment:* $F(-1) = 0, \Delta_{n-2}^-(\mu_0, x_0) = 0, F(1) > 0, \Delta_{n-2}^+(\mu_0) > 0, \Delta_l^\pm(\mu_0, x_0) > 0,$
$(-1)^{n-1} \sum_{k=1}^n \left((-1)^{n-k} \sum_{l=1}^k \left((-1)^{k-l} a_{l-1} \right) \right) > 0,$ *in which* $l = n - 4, n - 6, \ldots, 1$ *(or 2), when* n *is odd (or even), accordingly;*

(C_{32}) *transversality condition:* $\left. \frac{\partial \Delta_{n-2}^-(\mu, x)}{\partial \mu_j} \right|_{\mu = \mu_0} \neq 0, \sum_{i=1}^n a_{ij}'(-1)^{n-i} \neq 0,$ *where* $j = 1, 2$. *The term* a_{ij}' *denotes the derivative of* a_i *with respect to the bifurcation parameter* μ_j *at* $\mu = \mu_0$;

(C_{33}) *nonresonance condition:* $\cos\left(\frac{2\pi}{m}\right) \neq 1 - \frac{F_{\mu_0}(1)\Delta_{n-4}^-(\mu_0)}{4\Delta_{n-3}^+(\mu_0)},$ *in which* $m = 3, 4, 5, \ldots$ *and* $\Delta_k^\pm(\mu) = 1$ *if* $k \leqslant 0$.

Proof. (See [36]). The eigenvalue assignment condition demonstrates that the Jacobian matrix $J(\mu_0, x_0)$ possesses a singular real eigenvalue of -1, alongside a pair of complex conjugate eigenvalues whose magnitude is 1. This implies the presence of three eigenvalues positioned on the unit circle, with any additional eigenvalues (should they be present) residing within the unit circle. Furthermore, the criterion of transversality mandates that the complex conjugate eigenvalue pair intersects the unit circle at a non-zero velocity. □

Applying the above conditions (C_{31})-(C_{33}), we can obtain the existence conditions of flip-N-S bifurcation of the model (3.2) as

$$\begin{cases} y_1 \equiv \frac{(cb-d)adh^3(s,\alpha)}{(bc)} - \frac{2da((d+a+1)cb+ad^2)h^2(s,\alpha)}{(bc(ad+cb))} + \frac{4((d+1)cb+ad)h(s,\alpha)}{(bc)} - 8 = 0, \\ y_2 \equiv 2 - \frac{(cb-d)adh^3(s,\alpha)}{(bc)} + \frac{da((d+a+1)cb+ad^2)h^2(s,\alpha)}{(bc(ad+cb))} - \frac{((d+1)cb+ad)h}{(bc)} = 0, \\ y_3 \equiv \frac{(cb-d)adh^3(s,\alpha)}{(bc)} > 0, \\ y_4 \equiv \frac{(cb-d)adh^3(s,\alpha)}{(bc)} - \frac{da((d+a+1)cb+ad^2)h^2(s,\alpha)}{(bc(ad+cb))} + \frac{((d+1)cb+ad)h(s,\alpha)}{(bc)} > 0, \\ y_5 \equiv \frac{da((d+a+1)cb+ad^2)h^2(s,\alpha)}{(bc(ad+cb))} - \frac{4((d+1)cb+ad)h(s,\alpha)}{(bc)} + 12 > 0, \\ y_6 \equiv \frac{-3(cb-d)adh^2(s,\alpha)}{(bc)} + \frac{2da((d+a+1)cb+ad^2)h(s,\alpha)}{(bc(ad+cb))} + \frac{(-(d+1)cb-ad)}{(cb)} \neq 0, \\ y_7 \equiv \frac{1}{b^2c(ad+cb)^2}[-da(b^2((h^2(s,\alpha)+h(s,\alpha))d+ah(s,\alpha)+h(s,\alpha)-1)c^2 + 2 \\ \quad d(-1 + (h^2(s,\alpha)+h(s,\alpha))d)abc + d^2(-1 + (h^2(s,\alpha)+h(s,\alpha))d)a^2)h(s,\alpha)] \neq 0, \\ y_8 \equiv \frac{3(cb-d)adh^2(s,\alpha)}{(bc)} - \frac{4da((d+a+1)cb+ad^2)h(s,\alpha)}{(bc(ad+cb))} + \frac{(4(d+1)cb+4ad)}{(cb)} \neq 0, \\ y_9 \equiv \frac{1}{b^2c(ad+cb)^2}[d(2b^2((1/2h^2(s,\alpha)+h(s,\alpha))d+ah(s,\alpha)+h(s,\alpha)-2)c^2 \\ \quad +2d(-4 + (h^2 + 2h(s,\alpha))d)abcc + d^2(-4 + (h^2(s,\alpha)+2h(s,\alpha))d)a^2)ah(s,\alpha)] \neq 0. \end{cases} \tag{5.3}$$

The conditions specified in equation (5.3) are represented in Fig. 3. The shaded area signifies the parameter domain where all inequalities (y_3)-(y_5) are satisfied, while in the blank region, at least one inequality does not hold. These inequalities are represented by the colored lines in blue, magenta, and cyan, accordingly. The equations (y_1) and (y_2) are represented by red and green. The nonresonance conditions are illustrated by (y_6)-(y_9), but they do not appear in the first quarter of the (s-b) plane in Fig. 3. Notably, we have two intersection points, P_1 and P_2, between equations (y_1) and (y_2) in the shaded solution area. In accordance with Theorem 5.3, points P_1 and P_2 are identified as bifurcation points, meeting all the conditions specified in the semi-algebraic system (5.3).
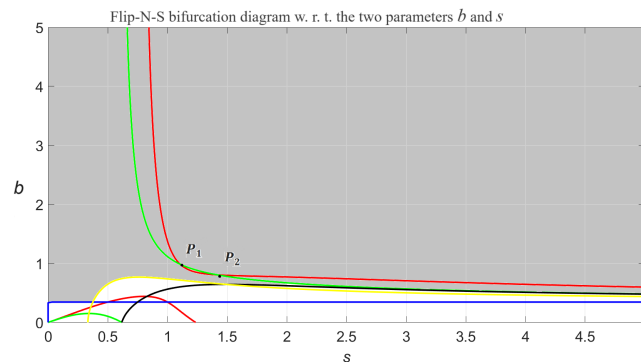
Figure 3: The conditions described in the semi-algebraic system (5.3) are exemplified for the values $r = 2, k = 2, \delta = 0.5, \gamma = 0.5, \beta = 0.725, \alpha = 0.99$, and $b \in (0, 2.5), s \in (0, 2.5)$.

6. Numerical simulations

In this part, we carry out numerical simulations to bolster the theoretical results discussed in the earlier Sections 4 and 5. Here, we introduce four scenarios, each with a different set of parameters of numerical simulations to illustrate the occurrence of N-S, flip, and fold bifurcations at the tumour-infected equilibrium point E_2 as well as the intersection between the flip and N-S bifurcations of the model (3.2). The parameters of fractional order α, the infection rate β, the burst size rate b, and the step size time s have been selected as critical bifurcation parameters to demonstrate their significant influence on our discrete-time model with fractional order (3.2). By selecting numerical biologically feasible parameter values, we obtain the following cases.

Case 1. Consider $r = 2, k = 1, \beta = 2, \delta = 0.5, b = 0.9, \gamma = 0.5$, and $s = 1.81$, and let the fractional order $\alpha \in (0, 0.99)$. Thus the model (3.2) has a tumour-infected equilibrium point $E_2(0.277, 0.38, 0.342)$ with $\mathcal{R}_0 = 3.6 > 1$.
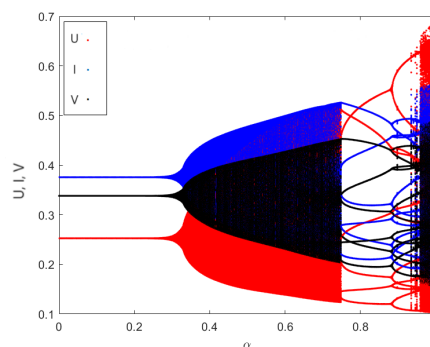

Figure 4: The N-S bifurcation diagram at E_2 when $\alpha \in (0, 0.99)$.

The occurrence of N-S bifurcation is shown in Fig. 4 when the fractional order parameter α varying into the region $(0, 0.99)$. It can be observed from Fig. 4 that E_2 is stable for $\alpha < 0.325$ and loses its stability through N-S bifurcation when $\alpha = 0.325$. Attracting closed invariant circle is observed in Fig. 4 when α passes the critical value 0.325. Chaotic regions appeared as α increases. Some phenomena of periodic orbits within the chaotic regions are clearly observed in Fig. 4. These recurrent cycles signal the presence of stable windows of periodicity or consistent oscillations within the tumour cell population arising from N-S bifurcation. From a biological standpoint, these oscillations could be seen as a diminishment of the tumour. The observations in Fig. 4 illustrate the reaction process that occurs after the initiation of viral therapy doses. A state of instability begins to appear in the cells as a result of the crazy increase in tumour cells. Of course, this requires taking the targeted virus treatment measures in our research. Fig. 4 shows the correlative increase between the spread of cancer cells and the therapeutic virus. The result of the interaction between them yields the expected infection within the tumour cells and then the transfer of a number of cells that were not infected to the infected ones. These observations are clearly shown in the chaotic regions of infected cells.

The phase portrait of the observations shown in Fig. 4 is depicted in Fig. 5. A stable steady state of E_2 is shown in Fig. 5 (a) for $\alpha = 0.3$. Initiating of an attracting closed circle is observed in Fig. 5 (b) when $\alpha = 0.325$. The phenomena of periodic-6 and 12 orbits observed within the chaotic regions are depicted in Figs. 5 (c)-(d) when $\alpha = 0.8$ and $\alpha = 0.891$, respectively. These phenomena of periodic orbits that appear within the chaotic regions explain the success of viral therapy in controlling the rampant spread of tumour cells. It is known that α-values change directly with the s-values. That explains the positive development in partial controlling of increasing tumour cells with the time increasing of the virus's work. However, this matter does not remain until the end, as it appears in Fig. 5 (e)-(f). The resurgence of tumour cell proliferation indicates why complete eradication of cancerous cells with viral therapy alone is not feasible, as noted in biological research [17, 26]. Mathematically, when comparing the outcomes (refer to Figs. 4 and 5) across varying values of α, it becomes apparent that the stability correlates with the fractional derivative's order.

(a) A stable steady state when $\alpha = 0.3$.

(b) An attracting closed invariant circle initiates when $\alpha = 0.325$.

(c) Periodic-6 orbits when $\alpha = 0.8$.

(d) Periodic-12 orbits when $\alpha = 0.891$.

(e) Periodic-8 orbits at E_2 when $\alpha = 0.94$.

(f) Chaos attractor regions at E_2 when $\alpha = 0.99$.
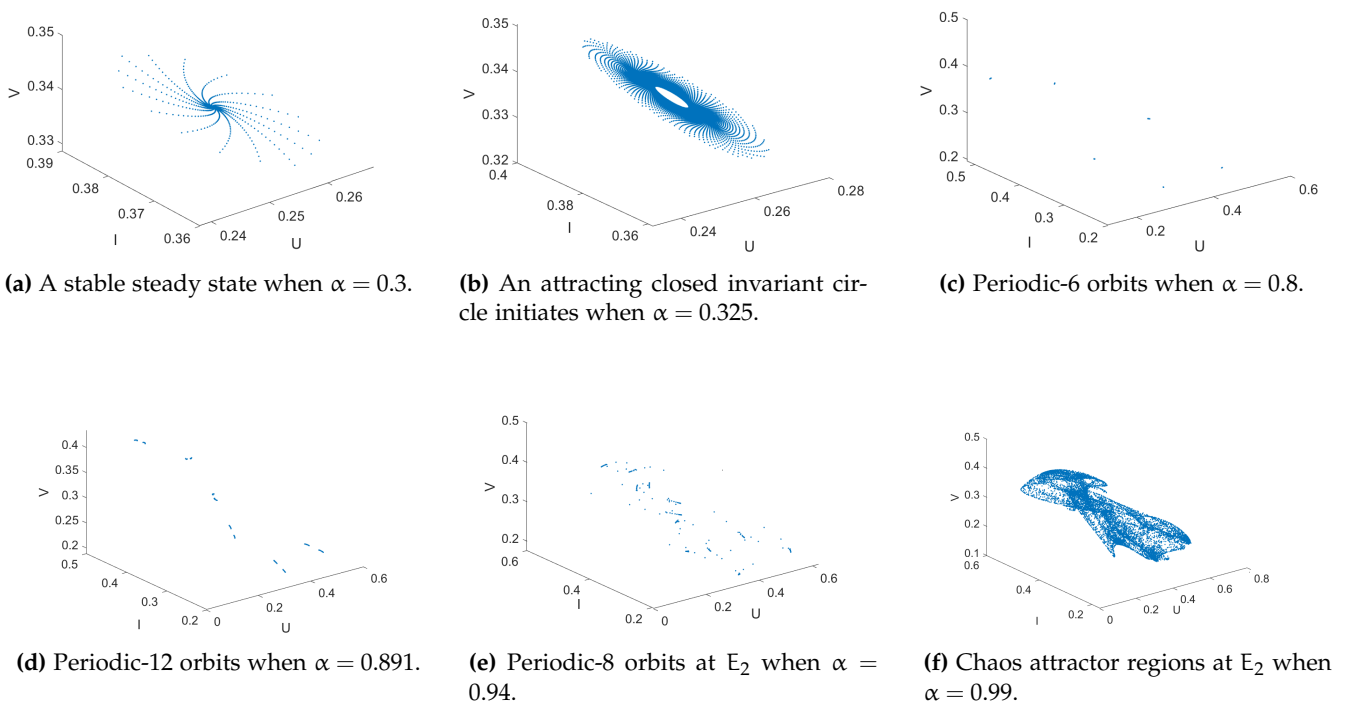
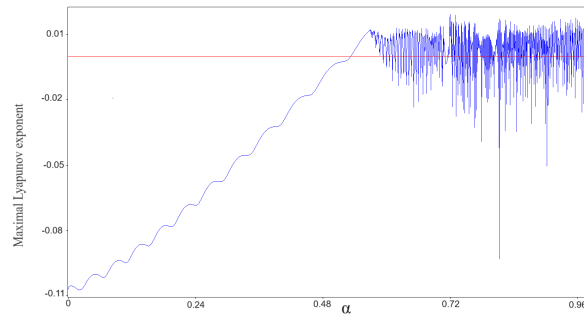**Figure 5:** The phase portrait of the model (3.2) corresponding to Fig. 4.

Figure 6: Maximal Lyapunov exponent corresponding to Fig. 4.

The positive Maximal Lyapunov exponent is a significant criterion for determining when a dynamical system is considered "chaotic". This generally suggests that the system is not stable and demonstrates chaotic behaviour. The maximal Lyapunov exponents related to Figure 4 are calculated in Figure 6. It shows some negative and positive Lyapunov exponent values, so there are stable fixed points or windows of a stable period located in the chaotic regions. Similar observations can be seen in Fig. 4 and Fig. 5 (e)-(f). In Fig. 6, the Lyapunov exponent values can be seen shifting from negative to positive approximately when $\alpha \approx 0.5$. This means an attracting invariant closed curve bifurcates from E_2 already shown in Fig. 5 (b). Chaotic regions are observed clearly in Fig. 6 with increasing of α-values.

Case 2. Consider $r = 2.7$, $k = 1$, $\delta = 0.5$, $b = 0.9$, $\gamma = 0.5$, $s = 1.3$, and $\alpha = 0.99$. The infection rate parameter β is selected as a bifurcation parameter to vary in the range of $(0.725, 0.9)$. In this range, a flip bifurcation appears in Fig. 7. Fig. 7 shows the occurrence of flip bifurcation at the equilibrium point E_2. Chaotic attractors to period-doubling route (flip bifurcation) along with intermittent periodic windows are clearly visible in the behavior of the model (3.2) with the change of the β-values in the range $(0.725, 0.795)$. It begins with chaotic regions within uninfected and infected tumour cells and with the apparent spread of the therapeutic viruses into the region of $(0.725, 0.795)$ in Fig. 7 as well. This is followed by stable periodic orbits or stable windows for all cells and the therapeutic virus as β-values increase. Fig. 7 shows the appearance of complete stability in all cells with increasing β values. This shows that under the specified conditions and values, viral therapy can completely stop the spread of cancer cells.
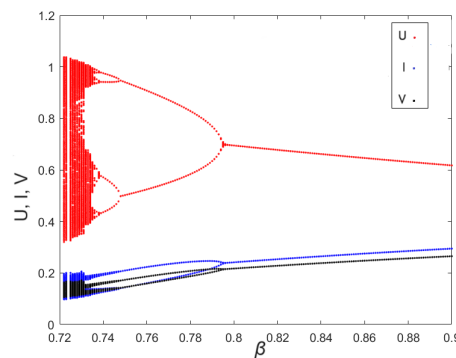

Figure 7: Flip bifurcation diagrams when $\beta \in (0.725, 0.9)$.

The phase portrait of the model (3.2) corresponding to Fig. 7 is depicted in Fig. 8. The chaotic regions due to the flip bifurcation appear in Fig. 8 (a) when $\beta = 0.726$. Fig. 8 (b)-(c) show the periodic-4 orbits and the periodic-2 orbits when $\beta = 0.7441$ and $\beta = 0.75$, respectively. A steady state equilibrium point starts with increasing β values (see Fig. 8 (d)). The Maximal Lyapunov exponent values corresponding to the observations in Fig. 7 are plotted in Fig. 9. It is noted that some Lyapunov exponent values are positive, confirming the existence of chaos in the system, while others are negative, confirming steady, and stable points.
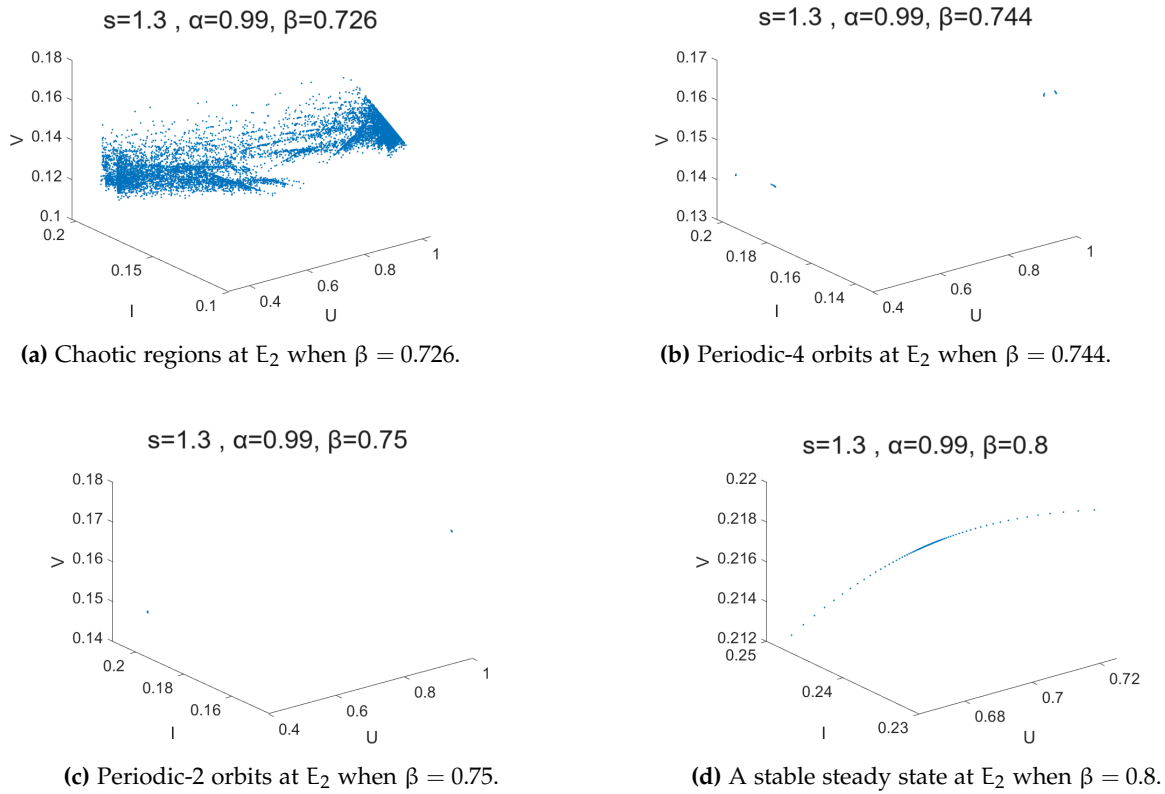
(a) Chaotic regions at E_2 when $\beta = 0.726$.

(b) Periodic-4 orbits at E_2 when $\beta = 0.744$.

(c) Periodic-2 orbits at E_2 when $\beta = 0.75$.

(d) A stable steady state at E_2 when $\beta = 0.8$.

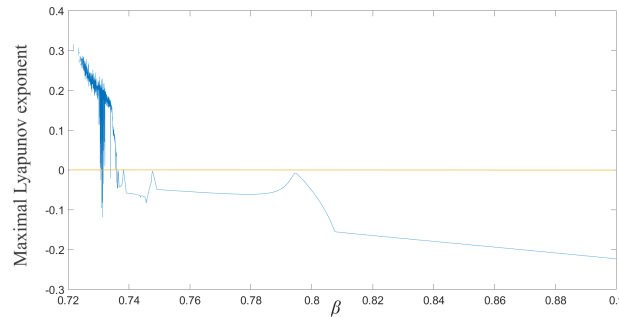**Figure 8:** The phase portrait of the model (3.2) corresponding to Fig. 7.

Figure 9: Maximal Lyapunov exponent corresponding to Fig. 7.

Case 3. Consider $r = 2$, $k = 1$, $\beta = 2$, $\delta = 0.5$, $s = 0.4726$, and $\alpha = 0.99$. Choose the burst size rate b as a bifurcation parameter to be varying in the range $(0, 2.1)$. Firstly, according to the analysis of the bifurcation section, the occurrence of the fold requires the fulfillment of the condition $F(1) = 0$. That is, by extension, it requires $\mathcal{R}_0 = 1$. This necessarily requires that $\gamma = b\delta c$, for all varying values of b into $(0, 2.1)$. The fixed values guarantee that the other conditions are satisfied to achieve a fold bifurcation when $b \in (0, 2.1)$. Fig. 10 shows fold bifurcation diagram at E_2 for $b \in (0, 2.1)$. From Fig. 10, we notice a slight disturbance in the stability of all cancer cells, and the virus begins when the basic reproduction number $\mathcal{R}_0$ exceeds the value of unity, with which the fold bifurcation begins to appear. Biologically, we notice an increase in virus virulence, accompanied by a simultaneous decrease in cancer cells. That is, as the size of the burst size increases, it results in greater replication of the virus. This is evident from the observed level of chaos within the viral population, which surpasses that found in cancer cells. Notably, the bifurcation diagram here does not indicate the complete eradication of cancer cells, but it demonstrates the possibility depending on the strength of the virus type.
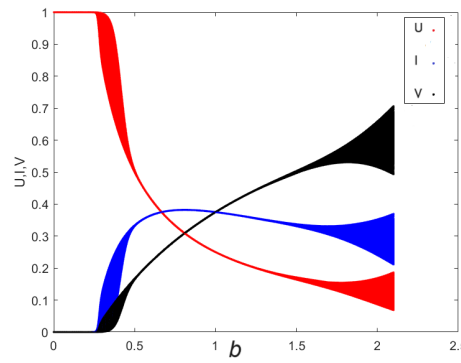
Figure 10: Fold bifurcation diagrams when $b \in (0, 2.1)$.

The phase portrait of observations in Fig. 10 can be shown in Fig. 11. In Fig. 11 (a), a steady state equilibrium point is depicted for $b = 0.21$. This indicates that the burst size of the virus has no influence on the dynamic behavior of the model (3.2). Subsequently, in Fig. 11 (b), we notice an insignificant change in the stability of the equilibrium point (see example $b = 1$). The equilibrium point E_2 loses its stability via fold bifurcation as b increases (see Fig. 11 (c) at $b = 2.1$).

(a) Steady state equilibrium at E_2 when $b = 0.21$.

(b) Unstable equilibrium at E_2 when $b = 1$.

(c) Chaotic situation at E_2 when $b = 2.1$.
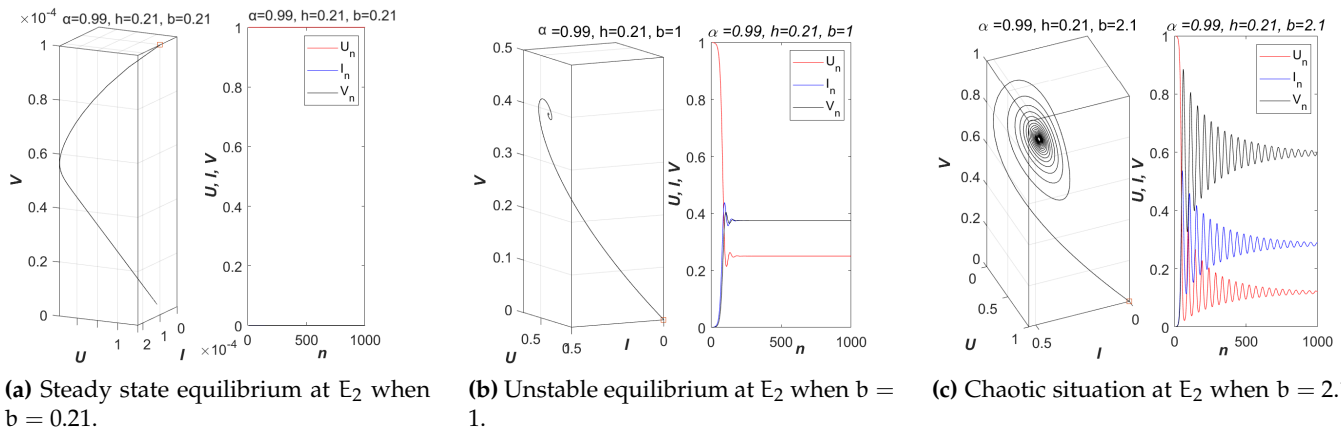
Figure 11: The phase portrait of the model (3.2) corresponding to Fig. 10.

Case 4. Consider $r = 2, k = 2, \delta = 0.5, \gamma = 0.5, \beta = 0.725$, and $\alpha = 0.99$. These fixed value parameters satisfy the semi-algebraic system (5.3). Solving the equality yields $y_1 = y_2$ as s and b are two variables yielding two critical points of Flip-N-S bifurcation (denoted as P_1 and P_2 in Fig. 3: $(s_*, b_*), (s_{**}, b_{**}) = (1.1026, 0.9889), (1.3969, 0.8131)$, respectively). The flip-N-S diagram of infected individuals of the cell population is depicted with $(s - b - I)$ plane in Fig. 12 when $b \in (1, 2.5)$ and $s \in (1.5, 2.5)$. In this case, we explore the implications of modulating two specific parameters within the context of virotherapy, a therapeutic intervention leveraging viruses to treat diseases. Our analysis reveals the emergence of two distinct bifurcations, specifically flip-N-S bifurcations, at P_1. Over time, the effect of viral blast size on the therapeutic process becomes more evident through infection of cancer cells, illustrating the correlation between blast size and time step size during the treatment process. Flip-N-S bifurcation emerges at E_2 close to P_1 when $b \in (0.1, 2.5)$ and $s \in (0.01, 1.2)$ (Fig. 12).
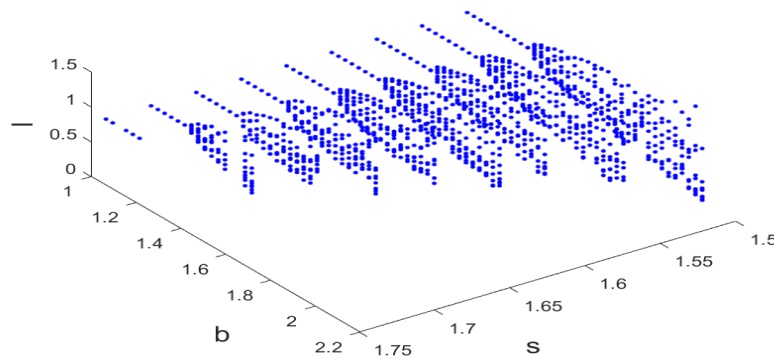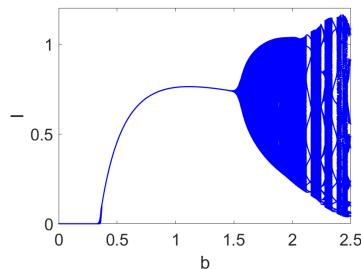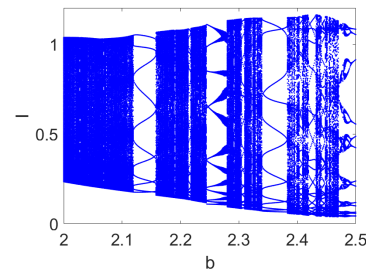
Figure 12: The Flip-N-S bifurcation diagram of the model (3.2) at E_2 in (s-b-I) plane when $b \in (1, 2.5)$ and $s \in (1.5, 2.5)$.

Fig. 13 (a) shows the bifurcation diagram in (b − I) plane at E_2 when $b \in (0.1, 2.5)$. An amplification is shown in Fig. 13 (b) to enhance the clarity of periodic orbits or stable windows within chaotic attractors. In Fig. 14 (a), the bifurcation diagram in the (s-I) plane at E_2 is shown at $s \in (0.01, 1.2)$. Fig. 14 (b) shows an amplification to improve the resolution of chaotic attractors followed by periodic orbits or stable windows. From Fig. 14, it can be seen that the replication of viruses increases with time. Figs 13 and 14 exhibit comparable patterns characterized by the bifurcation of periodic orbits transitioning to invariant curves, then evolving into hoping chaos attractors, quasi-periodic orbits as well as ultimately flipping chaos attractors.
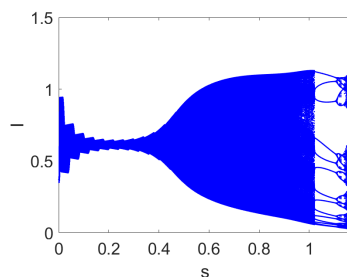

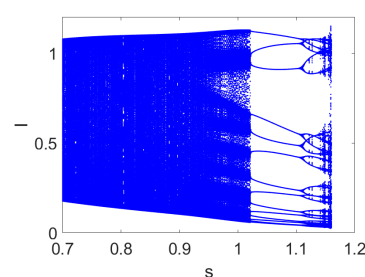
(a) Flip-N-S bifurcation in (b-I) plane.

(b) Amplification of Fig. 13 (a).

Figure 13: The Flip-N-S bifurcation diagram at E_2 when $b \in (1, 2.5)$.

(a) Flip-N-S bifurcation in (s-I) plane.

(b) Amplification of Fig. 14 (a).

Figure 14: The Flip-N-S bifurcation diagram at E_2 when $s \in (1.5, 2.5)$.

The phase portrait of the observations shown in Fig. 13 is depicted in Fig.15 (a)-(f) for various s and

b values. A stable equilibrium point E_2 appears in Fig. 15 (a) when ($b = 2.5, s = 0.4$). An invariant closed circle is shown in Fig. 15 (b) to show the beginning of the emergence of N-S bifurcation. Some interesting phenomena like Periodic-14-28-12 orbits within chaotic attractors when ($b = 2.5, s = 1.05$), ($b = 2.5, s = 1.117$), and ($s = 1.12, b = 2.26$), respectively, are shown in Figs. 15 (c)-(e). This indicates the formation of doubling periods (flip) inside the N-S bifurcation. Attracting chaotic sets appears in Fig. 15 (f) when ($s = 1.12, b = 2.57$). In this scenario, it is observed that Cases 1 and 3 exhibit consistency with regard to the partial success of the viral treatment. This is characterized by fluctuations transitioning from chaos to relative stability and then back to chaos, albeit of a lesser intensity than previously observed. Such patterns may suggest that this partial success has the potential to evolve into complete success of the treatment. In contrast, Case 2 demonstrates stability under specific conditions, despite an increase in viral infections.
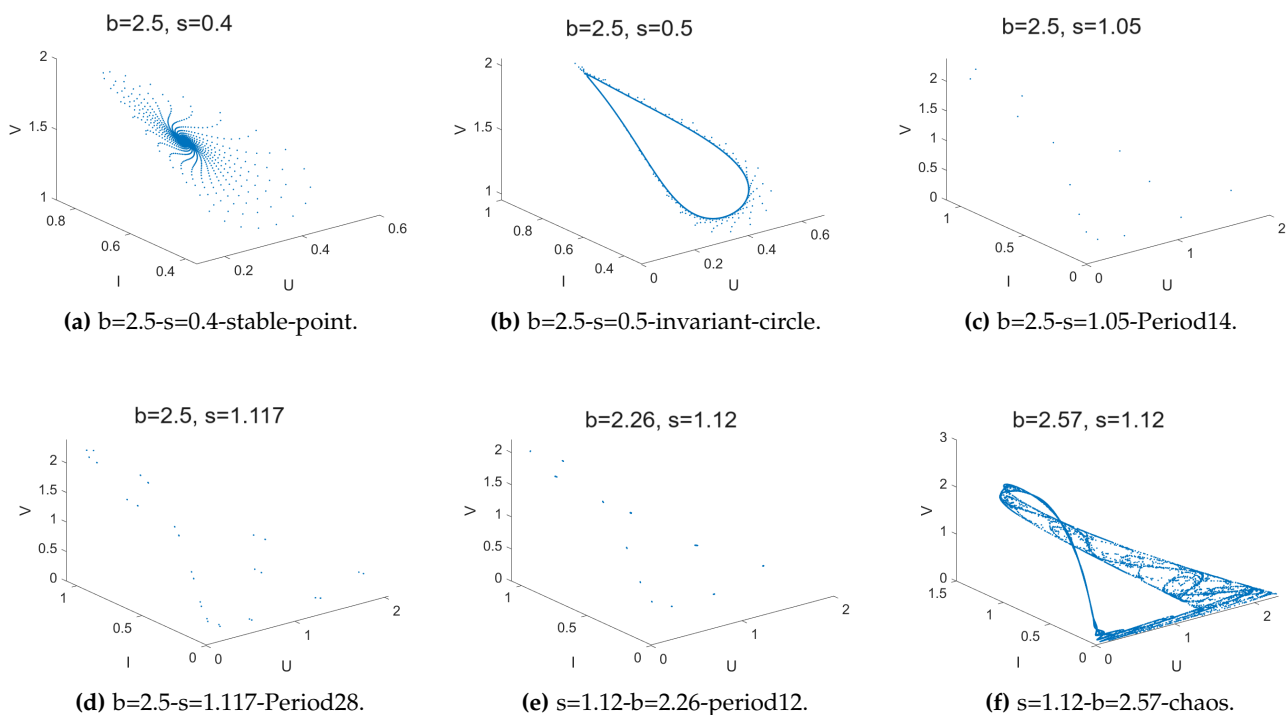

(a) b=2.5-s=0.4-stable-point.   **(b)** b=2.5-s=0.5-invariant-circle.   **(c)** b=2.5-s=1.05-Period14.

(d) b=2.5-s=1.117-Period28.   **(e)** s=1.12-b=2.26-period12.   **(f)** s=1.12-b=2.57-chaos.

Figure 15: The phase portrait of the model (3.2) corresponding to Figs. 13-14.

7. Conclusions

Virotherapy promises a qualitative and revolutionary transformation in the world of cancer treatment. Clinical studies investigating the application of oncolytic viruses in treating different cancer types have demonstrated notable decreases in tumour size and prolonged survival rates among patients [5, 6]. Given the significant therapeutic potential of this approach in combating cancer, there has been considerable interest in developing and examining mathematical models to advance our understanding of viral therapy, uncovering pivotal factors for its evolution. In the study presented, a novel discrete-time virotherapy model for cancer treatment, labeled as model (3.2), incorporating fractional order has been developed to enhance the framework previously established by Jenner et al. [13]. This model outlines how cancer cells and virus particles interact, specifically focusing on the virus's role in infecting and eradicating tumours. The existence of tumour-infected equilibrium point is investigated using the basic reproduction number $\mathcal{R}_0$. A detailed analysis of the local stability analysis of three equilibria is presented in this paper. The emergence of N-S, flip, and fold bifurcations, as well as the intersection between the flip and N-S bifurcations, is determined using algebraic criterion methods. As a result of the numerical simulations,

the parameters of the long memory characteristic of the fractional-order α, the infection rate β, the burst size rate b, and the step size time s have shown substantial dynamic behavior of the model (3.2). In the discrete-time model with fractional-order dynamics, it was demonstrated that the model is more stable due to the wider stability domain. Therefore, selecting the appropriate fractional order based on actual data can result in a more reliable model, since it integrates the memory effect and could potentially lower mistakes stemming from oversimplifications commonly found in traditional modelling techniques. Our model encompasses a broader range of scenarios, particularly those involving tumour remission. Under certain numerical conditions, virotherapy was capable of completely stabilizing the spread of cancer cells and eradicating the cancer. This represents a significant advancement compared to the research presented by Jenner et al. [13]. It was observed that an increase in $\mathcal{R}_0$ by a very small amount from the unity caused severe chaos resulting from the non-stop spread in tumour cells despite the proximity of the virus-free equilibrium point. Some phenomena of periodic orbits have been detected within the chaotic regions, which explains the existence of stable period windows or stable windows in the cancer cell population. These stable windows are biologically interpreted as an attenuation in tumourigenesis as a result of increased viral lysis within tumour cells. Our study concluded that the correlative increase between cancer cell proliferation and the therapeutic virus produced the expected infection within the cancer cells. Complete eradication of cancer cells using viral therapy alone is not impossible under special conditions. In future work, we will study the addition of the effect of immune cells in the case of oncolytic viral therapy. The purpose of future study is to infer the role of negative and positive immune responses in tumour cell proliferation during viral oncolytic therapy.

Acknowledgment

Funding

References

[1] M. A. M. Abdelaziz, A. I. Ismail, F. A. Abdullah, M. H. Mohd, *Bifurcations and chaos in a discrete SI epidemic model with fractional order*, Adv. Difference Equ., **2018** (2018), 1–19. 1

[2] M. A. M. Abdelaziz, A. I. Ismail, F. A. Abdullah, M. H. Mohd, *Codimension one and two bifurcations of a discrete-time fractional-order SEIR measles epidemic model with constant vaccination*, Chaos Solitons Fractals, **140** (2020), 14 pages. 3.1, 3.1, 5.2

[3] M. J. Ailia, S. Y. Yoo, *In vivo oncolytic virotherapy in murine models of hepatocellular carcinoma: a systematic review*, Vaccines, **10** (2022), 1–16. 1

[4] A. H. Alblowy, N. Maan, S. A. Alharbi, *Role of glucose risk factors on human breast cancer: A nonlinear dynamical model evaluation*, Mathematics, **10** (2022), 1–20. 1

[5] A. A. Al-Zaher, R. Moreno, C. A. Fajardo, M. Arias-Badia, M. Farrera, J. de Sostoa, L. A. Rojas, R. Alemany, *Evidence of anti-tumoral efficacy in an immune competent setting with an irgd-modified hyaluronidase-armed oncolytic adenovirus*, Mol. Ther., **8** (2018), 62–70. 1

[6] S. E. Berkey, S. H. Thorne, D. L. Bartlett, *Oncolytic virotherapy and the tumor microenvironment*, In: Tumor Immune Microenvironment in Cancer Progression and Cancer Therapy, Adv. Exp. Med. Biol., Springer, Cham, (2017), 157–172. 1

[7] H. Boutayeb, S. Bidah, O. Zakary, M. Rachik, *A new simple epidemic discrete-time model describing the dissemination of information with optimal control strategy*, Discrete Dyn. Nat. Soc., **2020** (2020), 11 pages. 1

[8] W. M. Chan, G. McFadden, *Oncolytic poxviruses*, Annu. Rev. Virol., **1** (2014), 191–214. 1

[9] B. S. Chhikara, K. Parang, *Global cancer statistics 2022: the trends projection analysis*, Chem. Biol. Lett., **10** (2023), 1–16. 1

[10] A. El-Sayed, S. Salman, *On a discretization process of fractional-order riccati differential equation*, J. Fract. Calc. Appl., **4** (2013), 251–259. 3.3

[11] M. Farman, A. Akgül, A. Ahmad, S. Imtiaz, *Analysis and dynamical behavior of fractional-order cancer model with vaccine strategy*, Math. Methods Appl. Sci., **43** (2020), 4871–4882. 3.1

[12] A. C. Filley, M. Dey, *Immune system, friend or foe of oncolytic virotherapy?*, Front. Oncol., **7** (2017), 1–17. 1

[13] A. L. Jenner, A. C. F. Coster, P. S. Kim, *Treating cancerous cells with viruses: insights from aminimal model for oncolytic virotherapy*, Lett. Biomath., **5** (2018), S117–S136. 1, 7

[14] P. Kumar, V. S. Erturk, A. Yusuf, S. Kumar, *Fractional time-delay mathematical modeling of oncolytic virotherapy*, Chaos Solitons Fractals, **150** (2021), 14 pages. 1

[15] X. Li, C. Mou, W. Niu, D. Wang, *Stability analysis for discrete biological models using algebraic methods*, Math. Comput. Sci., **5** (2011), 247–262. 4, 4.4, 5, 5.1.2

[16] A. C. J. Luo, *Regularity and complexity in dynamical systems*, Springer, New York, (2012). 4.1

[17] A. M. Malfitano, S. Di Somma, N. Prevete, G. Portella, *Virotherapy as a potential therapeutic approach for the treatment of aggressive thyroid cancer*, Cancers, **11** (2019), 1–21. 6

[18] J. Malinzi, *A mathematical model for oncolytic virus spread using the telegraph equation*, Commun. Nonlinear Sci. Numer. Simul., **102** (2021), 16 pages. 1

[19] C. E. Miller, *The endometrioma treatment paradigm when fertility is desired: a systematic review*, J. Minim. Invasive Gynecol., **28** (2021), 575–586. 1

[20] K. D. Miller, L. Nogueira, A. B. Mariotto, J. H. Rowland, K. R. Yabroff, C. M. Alfano, A. Jemal, J. L. Kramer, R. L. Siegel, *Cancer treatment and survivorship statistics, 2019*, CA Cancer J. Clin., **69** (2019), 363–685. 1

[21] H. Murphy, H. Jaafari, H. M. Dobrovolny, *Differences in predictions of ode models of tumor growth: a cautionary example*, BMC Cancer, **16** (2016), 1–10. 1

[22] W. Niu, J. Shi, C. Mou, *Analysis of codimension 2 bifurcations for high-dimensional discrete systems using symbolic computation methods*, Appl. Math. Comput., **273** (2016), 934–947. 5, 5.3

[23] E. Ratajczyk, U. Ledzewicz, H. Schättler, *Optimal control for a mathematical model of glioma treatment with oncolytic therapy and TNF-α inhibitors*, J. Optim. Theory Appl., **176** (2018), 456–477. 1

[24] L. A. Santry, J. P. van Vloten, J. P. Knapp, K. Matuszewska, T. M. McAusland, J. A. Minott, R. C. Mould, A. A. Stegelmeier, P. P. Major, S. K. Wootton, J. J. Petrik, B. W. Bridle, *Tumour vasculature: friend or foe of oncolytic viruses?*, Cytokine Growth Factor. Rev., **56** (2020), 69–82. 1

[25] E. Shirbhate, R. Veerasamy, S. H. S. Boddu, A. K. Tiwari, H. Rajak, *Histone deacetylase inhibitor-based oncolytic virotherapy: A promising strategy for cancer treatment*, Drug Discov. Today, **27** (2022), 1689–1697. 1

[26] J. d. Sostoa, V. Dutoit, D. Migliorini, *Oncolytic viruses as a platform for the treatment of malignant brain tumors*, Int. J. Mol. Sci., **21** (2020), 1–21. 1, 6

[27] Y. R. Suryawanshi, A. J. Schulze, *Oncolytic viruses for malignant glioma: on the verge of success?* Viruses, **13** (2021), 1–25. 1

[28] C. A. Valentim, J. A. Rabi, S. A. David, *Fractional mathematical oncology: On the potential of non-integer order calculus applied to interdisciplinary models*, Biosystems, **204** (2021). 3.1

[29] C. A. Valentim Jr, N. A. Oliveira, J. A. Rabi, S. A. David, *Can fractional calculus help improve tumor growth models?* J. Comput. Appl. Math., **379** (2020), 15 pages. 1

[30] P. Van den Driessche, J. Watmough, *Further notes on the basic reproduction number*, Springer, Berlin, **1945** (2008), 159–178. 2

[31] B. D. Weinberg, J. Gao, *Polymer implants for intratumoral drug delivery and cancer therapy*, CRC Press, (2020). 1

[32] G. Wen, *Criterion to identify Hopf bifurcations in maps of arbitrary dimension*, Phys. Rev. E (3), **72** (2005), 4 pages. 5, 5.1

[33] G. Wen, S. Chen, Q. Jin, *A new criterion of period-doubling bifurcation in maps and its application to an inertial impact shaker*, J. Sound Vib., **311** (2008), 212–223. 5, 5.1.2, 5.2

[34] D. Wodarz, *Gene therapy for killing p53-negative cancer cells: use of replicating versus nonreplicating agents*, Hum. Gene Ther., **14** (2003), 153–159. 1

[35] T. Yamada, Y. Hamano, N. Hasegawa, E. Seo, K. Fukuda, K. K Yokoyama, I. Hyodo, M. Abei, *Oncolytic virotherapy and gene therapy strategies for hepatobiliary cancers*, Curr. Cancer Drug Targets, **18** (2018), 188–201. 1

[36] S. Yao, *New bifurcation critical criterion of flip-Neimark-Sacker bifurcations for two-parameterized family of n-dimensional discrete systems*, Discrete Dyn. Nat. Soc., **2012** (2012), 12 pages. 5, 5.3, 5.2.1

[37] Y. Zhou, J. W. He, *A cauchy problem for fractional evolution equations with hilfer's fractional derivative on semiinfinite interval*, Fract. Calc. Appl. Anal., **25** (2022), 924–961. 3.1